CrossMark

Performance of Limestone Calcined Clay Cement (LC^3) with various kaolinite contents with respect to chloride transport

Hamed Maraghechi · Francois Avet ⃝ · Hong Wong · Hadi Kamyab · Karen Scrivener

Abstract The durability of mortar and paste mixtures with respect to chloride ion ingress was investigated for binary blends of Portland Cement Calcined Clay, and ternary systems of Limestone Calcined Clay Cement (LC^3). Five clays from various sources with different kaolinite content (17–95%) were studied. The main factor controlling the diffusivity of LC^3 systems was found to be the kaolinite content of the clay. Resistance to chloride ingress increased to intermediate levels of kaolinite content and then stabilized. An intermediate kaolinite content of around 50% resulted in two orders of magnitude reduction in diffusivity compared to PC, indicating that the use of high grade (expensive) clays is not necessary to obtain good durability. The chloride binding capacity and distribution of bound chloride between Friedel's salt and C–A–S–H were quantified for the different systems at fixed water to binder ratio of 0.5. The chloride binding capacity appeared to be a minor factor compared to the porosity refinement in the improved durability of LC^3 systems.

Keywords Calcined clay · Limestone · Kaolinite · Chloride diffusion · Phase assemblage · Supplementary cementitious materials

1 Introduction

The production of Portland cement (PC) is the major source of CO_2 emissions associated with concrete materials. Due to the very large volumes of cementitious materials used (around 50% or all manufactured materials), it is estimated to be responsible for 6–8% of global anthropogenic greenhouse gas emissions [1, 2]. This originates mainly from decomposition of limestone during the formation of clinker and burning of fossil fuels in cement kilns. Global population growth is leading to increasing demand for cement. To satisfy this demand, while minimizing CO_2 emissions, the most viable approach is to employ supplementary cementitious materials (SCMs) as partial cement replacement. The global availability of conventional SCMs such as slag, fly ash, and silica fume is limited (only around 15% of cement production worldwide) and is declining in proportion to the demand for cement. Kaolinite clays, on the other hand, are abundant in Earth's crust [3]. Research on the use

H. Maraghechi · F. Avet (✉) · K. Scrivener
Laboratory of Construction Materials, EPFL STI IMX LMC, Station 12, 1015 Lausanne, Switzerland
e-mail: francois.avet@epfl.ch

H. Wong
Department of Civil and Environmental Engineering, Imperial College London, 228D Skempton, London SW7 2AZ, UK

H. Kamyab
Sustainable Materials Management Unit, Flemish Institute for Technological Research (VITO NV), Boeretang 200, 2400 Mol, Belgium

of kaolinitic clays as a cementitious component in concrete has increased in the last few years. The 1st and 2nd International Conferences on Calcined Clays for Sustainable Concrete [4, 5] brought together much ongoing research.

Most deposits of kaolinite clays are not pure, and contain other phases, which can be considered as impurities such as quartz, iron and titanium oxides, calcite and other types of clays [1]. Recent studies, as well as the current work, have shown that the use of calcined clays with low or intermediate purity (i.e., kaolinite content) lead to excellent concrete properties [6]. The use of intermediate grade kaolinite clays is more practical due to widespread availability at low cost, compared to high-grade kaolinite clays used to make "pure metakaolin", which are expensive. Clays must be calcined prior to their use in concrete to form the highly reactive amorphous metakaolin phase (AS_2) by dehydroxylation of crystalline kaolinite [7]. The optimum calcination temperature for kaolinitic clay is in the range 750–850 °C [8, 9].

The most important durability concern for concrete infrastructure is corrosion of steel reinforcement due to the ingress of chloride ions (e.g., from sea water or de-icing salts). The rate and extent of ion transport in concrete is influenced by both the physical pore structure of concrete at nano and micro scales, and the chemical and physical binding of chloride ions to the hydrates, specifically AFm phases and C–A–S–H. Therefore, understanding and quantifying physical and chemical characteristics of concrete components, made using new cementitious materials is essential to ensure good durability. Generally, it is known that the use of SCMs improves the resistance of concrete to ion transport, mainly attributed to the refinement of porosity [10]. In addition, the phase assemblage of hydrates is altered, with consequent changes—usually improvement- of the chloride binding capacity [11, 12].

The chemical binding of chloride ions by reaction with AFm phases has been documented extensively in the past. For PC systems, at low Cl concentrations (≤ 0.2 M), the formation of Kuzel's salt $3CaO.Al_2O_3 \cdot 1/2CaSO_4 \cdot 1/2CaCl_2 \cdot 11H_2O$ from AFm monosulfoaluminate is thermodynamically predicted, and at increasing Cl concentrations, Friedel's salt $3(CaO) \cdot Al_2O_3 \cdot CaCl_2 \cdot 10H_2O$ formation occurs [13]. In the presence of limestone and aluminates (from cement or clay), hemi- and monocarboaluminate AFm phases form [14, 15]. In the presence of chloride ions hemi- and monocarboaluminate AFm phases progressively convert to Friedel's salt. Thomas et al. [16] found an almost linear relationship between the amount of bound chloride and the Friedel's salt formed. In addition to the chemical binding, chloride ions are also physically adsorbed on C–A–S–H surface [17]. The physical adsorption of chloride on C–A–S–H depends on its composition: the lower Ca/Si in cements with SCMs is claimed to decrease the adsorption of chloride [18, 19]. In systems containing calcined clays, the Ca/Si ratio of the C–A–S–H is lower and there is a higher uptake of Al in C–A–S–H structure, seen by ^{29}Si MAS NMR analysis [20] or by SEM–EDX [21]. In addition, the type of salt (e.g., NaCl vs. $CaCl_2$), and pore solution pH may influence the chloride binding capacity of C–A–S–H [18, 22, 23].

There have been several studies on the durability of cementitious materials containing calcined kaolinite clay, either as binary or ternary (LC^3) blends [24–26]. Shi et al. [23, 27] used pure metakaolin in binary PC-calcined clay or ternary LC^3 blends with 35% replacement level, with the clay/limestone ratio of 4. Significant improvement in the resistance to chloride transport of mortars was reported. It was also observed that monocarboaluminate and strätlingite transform into Friedel's salt, but that, from the total chloride diffused into mortars, less than 5–10% was bound into Friedel's salt [23]. The distribution of chloride between Friedel's salt, C–A–S–H and free chloride was quantified in PC-metakaolin blends [27], and it was concluded that almost all bound chloride was chemically bound to Friedel's salt and not physically adsorbed on C–A–S–H.

This study investigates the durability characteristics of ternary mixtures PC Limestone Calcined Clay Cement (LC^3 cement, with 50% replacement) and binary blends of PC-calcined clay (PPC cement, with 30% replacement) with regards to chloride ion transport. While most past research focused on the use of high grade clays (i.e., clays with high kaolinite content, or metakaolin), we studied properties of concrete and paste mixtures with clays of different kaolinite content. In addition to chloride ingress, the binding characteristics of both binary mixes of Portland cement and calcined clay (PPC) and ternary mixes of Portland cement, calcined clay and limestone (LC^3) were studied at fixed water to binder ratio of 0.5.

The relative influence of binding and porosity on chloride transport is then investigated.

2 Materials

The cementitious materials used in this study included a type I ordinary Portland cement (CEM-I 42.5R), limestone, and five kaolinitic clays obtained from different sources worldwide, with the main characteristics presented in Table 1. Clays #2, #3 and #5 were calcined at around 800 °C for 1 h in a high temperature furnace (Borel FP1100), whereas clays #1 and #4 were received as calcined. The kaolinite content of clays was determined by Thermogravimetric Analysis (TGA). As it can be seen in Table 1, a wide range of clay compositions and calcined kaolinite contents was used. Quartz was used to represent clay material with 0% kaolinite content. The values of d_{v50} were obtained using laser diffractometer analysis (Malvern Mastersizer), and the specific surface was measured by

nitrogen adsorption (Micromeritics Gemini) using BET model.

In addition to a reference PC system, two series of blends (Table 2) were prepared: binary PC-calcined clay blends where PC was replaced by 30% of calcined clay (referred to as PPC-30) and ternary blends of PC Limestone Calcined Clay Cement with a clinker content of 50% (referred to as LC^3-50). PPC-30 blends were prepared with clays #1 and #4. Ternary LC^3-50 blends were made with all the five calcined clays, with the calcined clay to limestone ratio of 2:1, which was shown to give the best compressive strength development [7]. The commercial cement used in this study was properly sulfated for hydration alone. However, due to the presence of calcined clay with significant amount of aluminates, 2 wt% gypsum (> 98% purity) was added to the PPC-30 and LC^3-50 blends to give properly sulfated systems, as detailed in [28].

Both mortar and paste mixtures were prepared using a water to binder ratio of 0.5. To ensure similar workability to the PC systems (16 ± 2 cm on mortar,

Table 1 Properties of the cementitious components used in this study

	Cement	Limestone	Quartz	Clay #1	Clay #2	Clay #3	Clay #4	Clay #5
Origin	–	–	–	North America	South Asia	Southeast Asia	South Asia	South Asia
Calcination method	–	–	–	Flash	Static	Static	Rotary kiln	Static
Calcined kaolinite content (wt%)	–	–	–	95.0	79.4	50.3	41.9	17.0
Dv_{50} (μm)	8.4	7.2	11.2	5.1	5.3	10.9	7.8	5.8
BET surface (m^2/g)	0.9	1.8	1.2	9.6	15.3	45.7	9.2	18.7
SiO_2 (wt%)	19.3	0.1	99.8	52.0	51.8	44.9	53.5	68.4
Al_2O_3 (wt%)	5.7	–	–	43.8	42.4	32.3	34.8	17.5
Fe_2O_3 (wt%)	3.6	–	–	0.3	1.9	15.4	3.3	8.9
CaO (wt%)	63.6	55	–	–	0.1	1.3	0.1	0.6
MgO (wt%)	1.6	0.2	–	–	0.1	0.8	0.1	0.7
SO_3 (wt%)	3.2	–	–	0.1	–	0.1	–	–
Na_2O (wt%)	0.2	0.1	–	0.3	0.1	0.4	0.2	0.1
K_2O (wt%)	1.2	–	0.1	0.1	0.1	0.2	0.2	2.3
TiO_2 (wt%)	0.3	–	–	1.5	2.4	2.4	2.3	0.8
P_2O_5 (wt%)	0.2	–	–	0.2	0.1	0.4	0.2	0.1
MnO (wt%)	0.1	–	–	–	–	0.1	–	–
Others (wt%)	0.3	–	–	0.1	0.2	0.2	–	0.2
LOI (wt%)	0.8	42.6	0.1	1.5	1.0	1.7	4.7	0.5

Table 2 Mix composition (wt %) of PC, PPC30 and LC^3-50 blends

	Clinker	Anhydrite	Calcined clay	Limestone	Gypsum
PC	93.2	5.9	–	–	–
PPC30	64.5	4.1	29.4	–	2.0
LC^3-50	50.6	3.3	29.4	14.7	2.0

and 13 ± 2 cm on paste by mini-cone test), a poly-carboxylate superplasticizer was employed. The amount of superplasticizer added to the water increased with the calcined kaolinite content of the clay; up to 0.6% of binder content for mortars and 1.2% of binder content for pastes.

Mortar mixtures were prepared in accordance with EN 196-1 procedure and cast in cylindrical (110 mm diameter—300 mm height) and cubic (40 mm-side) molds. After 24 h of curing in sealed condition, specimens were demolded and stored in a fog room (RH > 95%). The compressive strength of mortar cubes was measured according to EN-196-1 at different ages. After 28 days of curing, the mortar cylinders were sawn on their diameter into two halves, epoxy coated on all surfaces except the sawn cut face and submerged in 3 wt% NaCl solution (equivalent to 0.51 M). The solution was renewed every two weeks during the first two months, then every month. After 1 and 2 y of exposure, the profiles of total chloride were obtained in accordance with ASTM-C1152 procedure, where ground mortar samples from incremental depths were dissolved in nitric acid, followed by titration using silver nitrate solution. The PPC-30 and LC^3-50 mixtures with 0 wt% (i.e., LC^3 with quartz) and 41.9 wt% kaolinite content were not exposed to the ponding solution.

Paste samples were prepared by initially blending the powders and mixing with distilled water (w/solid = 0.5) for 2 min at 1600 RPM. Fresh paste mixtures were cast in small plastic containers (30 mm diameter–50 mm height), cured for 24 h in sealed conditions, followed by curing under saturated lime water for 28 d. In a similar approach to the mortar ponding experiments, after cutting away 10 mm from the surface of the paste cylinders, the sides were coated with epoxy and exposed to 3% NaCl solution. After 6 and 18 m of exposure, the paste samples were removed from the solutions, and dry saw cut perpendicular to the exposed surface, to have a surface on

which the chloride gradient could be measured. The paste samples were then ground flat using sand paper (SiC #1200), with attention being made to ensure grinding was executed in a direction perpendicular to the diffusion direction to avoid contamination (Fig. 1). The samples were then freeze dried and the cut surfaces were analyzed using micro X-ray fluorescence (μ-XRF, Edax Ametek Orbis PC). The sample surface was irradiated using a focused X-ray beam causing element excitation and subsequent emission of characteristic X-rays (fluorescence). These emissions were detected and processed using energy-dispersive spectrometry (EDS) to obtain information concerning the type and quantity of the elements present. Analysis was carried out using a 30 μm spot size at 35 kV beam voltage, 30% dead time, 300 s live acquisition time and 12.8 μs time constant. A 25 μm aluminum filter was employed to improve the detection of chlorine by removing overlapping rhodium spurious peaks. At least 10 points were measured per depth increment of 1–2 mm. The conditions of the experiments were slightly different at 6 and 18 months, and therefore the total number of X-ray counts were slightly different between the two ages. Further information on the use of μ-XRF to
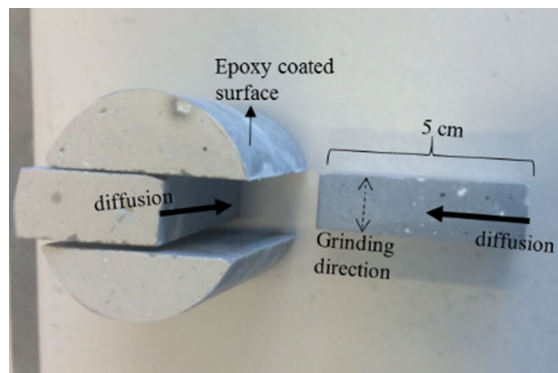
Fig. 1 μ-XRF sample preparation

analyze chloride transport in cementitious materials can be found in [29].

The chloride binding capacity and the interactions of NaCl solution with paste mixtures were studied. After the paste samples were cured for 28 d, they were broken into small pieces (0.5–1.0 mm), and dried in vacuum under low RH conditions, following a procedure described in [7]. The dried paste pieces, as well as one thin dried paste slice (1.0 mm thickness with 30 mm diameter) were submerged in NaCl solutions of 0.1–2.0 mol/L concentration, as well as a reference deionized water. The solution volume to solid ratio was kept at 4 cm^3/g. The slice in each container was used for characterization purposes, as explained below. After 5 months of exposure, when the stabilization of NaCl concentration was achieved, the chloride concentration of each solution was carefully measured using $AgNO_3$ potentiometric titration to acquire the amount of bound and free chloride. No pH adjustment was made to the solution in which the isotherms were measured so the findings of this study are valid only for the conditions explained here, as discussed later.

X-ray powder diffraction (XRD), coupled with Rietveld refinement analysis, was employed to study and quantify the phase assemblage of paste samples after exposure to NaCl solutions or water. A PANalytical X'Pert Pro MPD diffractometer in a θ–θ configuration using Cu-Kα source (λ = 1.54 Å) with a fixed divergence slit size of 0.5° was employed. To have a better identification and quantification of Friedel's salt, an equivalent time per step of 1 min was used, with a step size of 0.0167°2θ, scanned from 5° to 40° only. To determine the reaction degree of metakaolin needed for quantifying the amount of C–A–S–H, the XRD results were coupled with a mass balance approach as explained in [30].

To find the elemental composition of C–A–S–H, scanning electron microscopy, coupled with energy dispersive spectroscopy (SEM–EDS) analysis was employed following Rossen's method [31]. Paste samples that were exposed to either water or 2 M NaCl solution were dried using solvent exchange method and impregnated with a low viscosity epoxy resin. This drying method was assumed to remove only the free chloride, but not the chemically and physically bound chloride. Through successive grinding and polishing, using diamond abrasives down to 1 μm size, a flat surface was exposed for the analysis.

Carbon-coated polished sections were prepared and studied using a FEI quanta 200 SEM, equipped with a W-filament operated at an accelerating voltage of 15 kV. Over 200 points per sample were measured to find the average composition of C–A–S–H, and the amount of chloride in C–A–S–H.

Mercury intrusion porosimetry (MIP) (Porotec GmbH Pascal 140–440 instruments), up to a maximum pressure of 400 MPa was used to measure the distribution of pore entry sizes of the pastes dried by solvent exchange as above. A contact angle of 120 °C was used for all experiments. In addition to the water cured paste samples, selected mixtures were analyzed after exposure to 2 M NaCl solution to see if the combination of chloride ions affected the porosity of the pastes. Those mixtures included PC as well as LC^3 prepared using clays with 17, 50 and 95% kaolinite.

3 Results and discussion

3.1 Compressive strength

Figure 2a shows the compressive strength development for LC^3-50 and PC mortars. While the 1 day strength of PC was higher than all LC^3-50 systems, after 3 days of curing the strength of LC^3-50 mortar with a pure clay (95% kaolinite) was comparable to PC. After 7 days, all LC^3-50 mortars, that were made using clays with 40% kaolinite content and higher showed comparable or even higher strength than PC. At 28 and 90 days of curing, all LC^3-50 mortars, except the one made using very low kaolinite content (17%) attained higher strength than PC. The mortars with 41.9, 50.3, 79.4 and 95.0% kaolinite content showed 9, 9, 27 and 34% higher strength at 28 days than PC, respectively.

Figure 2b compares the strength of LC^3-50 mortars with PPC-30 mortars made using the same type of clay. The PPC-30 mortars showed comparable strength to LC^3-50 ones up to 7 days, and somewhat higher strengths at 28 and 90 days.

3.2 Chloride ion ingress

The extent of chloride ion ingress in mortar samples after one and two years of exposure to 3 wt% (0.51 M) NaCl solution is shown in Fig. 3. The LC^3-50 mortar with low kaolinite content (17%) showed comparable
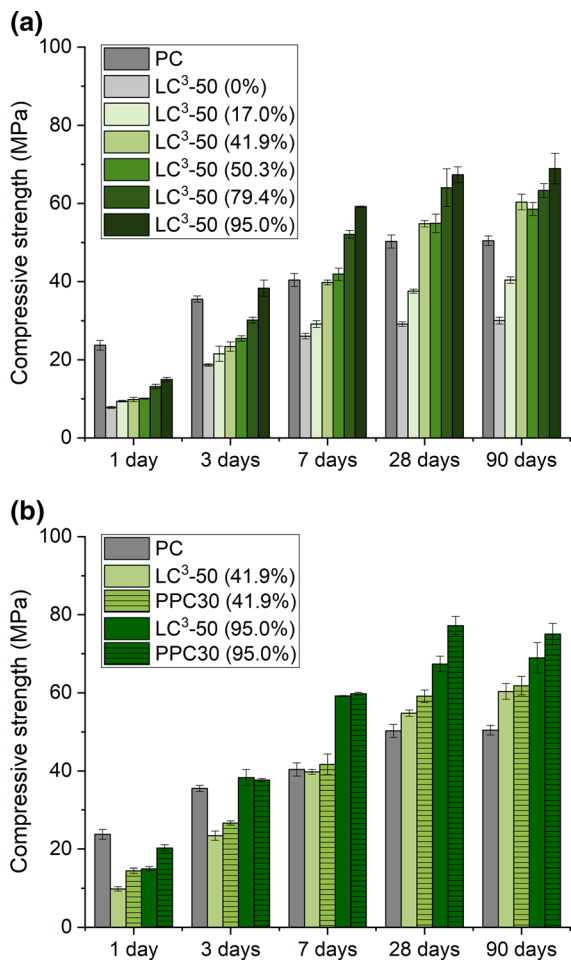
(a)

(b)

Fig. 2 Compressive strength of LC³-50 mortars as a function of clay grade and age (**a**); comparison of PPC-30 vs LC³-50 mortars prepared using the same clay (**b**)
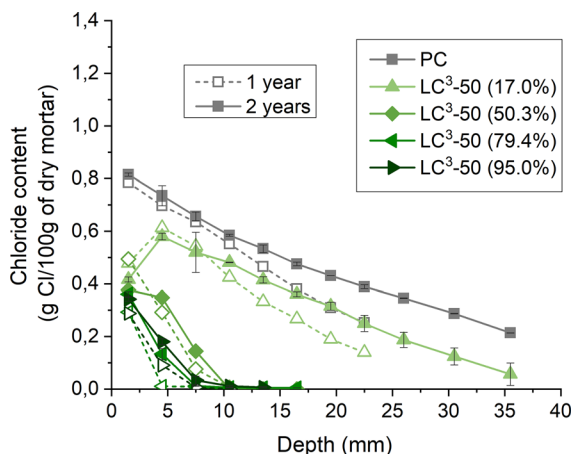

Fig. 3 Total chloride profiles for PC and LC³ mortars after 1 and 2 years of exposure to 3% NaCl ponding solution

chloride profile to that of PC, despite the replacement of cement by a material with only 17% active SCM (83% filler). All other LC³-50 blends had much improved the chloride resistance compared to PC. The depth of chloride ingress in LC³-50 mortars that were made by using clays with 50% kaolinite content and higher were much lower than that of PC. After 2 years of exposure, chloride penetration was deeper than 40 mm in PC mortars, while in LC³-50 mixtures (of 50% and higher kaolinite content), chloride ions reached a depth of about 10 mm. It is interesting to note that the chloride content measured at the top surface of the samples were higher for PC, which may indicate that PC has a higher binding capacity than the LC³-50 blends. However, the lack of detailed information at the exposed surface limits firm conclusions. Shi et al. [23] quantified the chloride content at 0.5 mm and 1.5 mm depth and found that the chloride content was significantly increased for a ternary blend of calcined clay and limestone and it reached values close to the reference PC blend.

Profiles of total chloride content measured using μ-XRF in paste samples after 6 and 18 months of exposure are plotted in Fig. 4. The results for LC³-50 systems agree well with those of the mortars presented in Fig. 3. Only LC³-50 (0%)—the system with quartz-showed worse resistance to chloride transport than PC, which is, of course, due to 50% dilution of clinker with quartz and limestone. LC³-50 (17%) showed similar profile to PC. At 18 months, chloride was detected through the whole sample for PC, LC³-50 (0%) and LC³-50 (17%) systems, as the depth of the samples were limited to 50 mm. All other LC³-50 pastes showed much improved resistance against ingress of chlorides compared to PC paste. The improvement increased with increasing the grade of the clay, but in general, there is not a huge gain achieved from using higher grade calcined clays with 79.4% and 95.0% of calcined kaolinite, compared with LC³-50 (50.3%) and LC³-50 (41.9%) systems. When LC³-50 systems are compared to PPC-30, with the same clays type, similar, or slightly improved behavior was observed in LC³-50 systems, as shown in Fig. 4b and d.

A better spatial resolution was obtained by μ-XRF compared with acid dissolution and titration method. This binding capacity from the top surface will be further discussed and compared with binding isotherm results later in the chloride binding part of this paper.
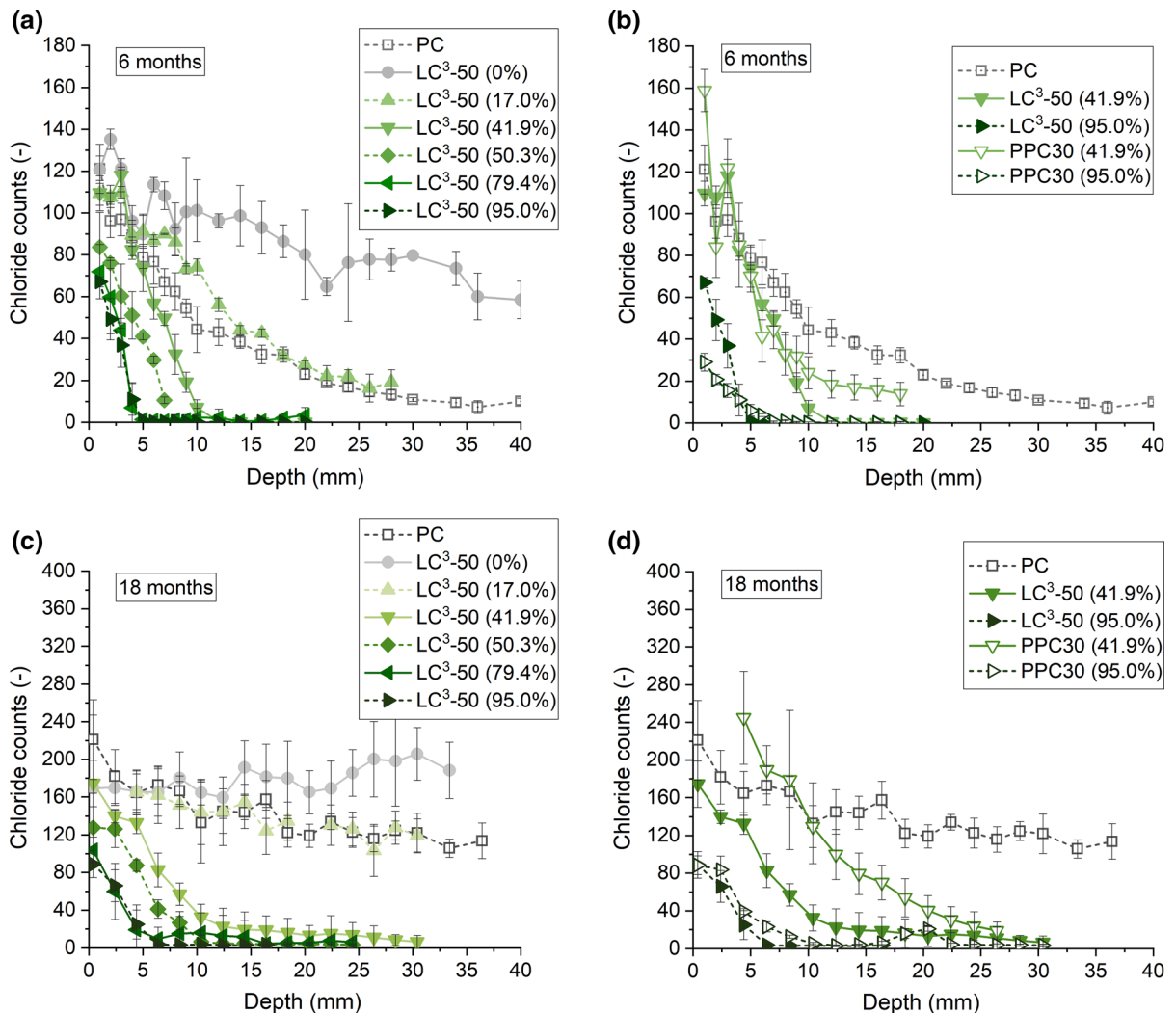
Fig. 4 Profiles of total chloride for pastes measured using μ-XRF after 6 (**a**, **b**) and 18 months (c,d) of exposure to 3 wt% NaCl solution

As noted before, the measurements at 6 months and 18 months were conducted using different equipment with slightly different experimental parameters, and therefore the number of counts between the two ages cannot be compared to each other. The purpose of the measurement; however, was to obtain the extent of diffusion and the shape of the profile, for calculation of the diffusivity coefficient. The apparent diffusion coefficient values calculated from the ponding tests on mortar and on paste were calculated from the total chloride content, using Fick's 2nd law of diffusion according to ASTM C1556. The values are reported in Fig. 5. The apparent diffusion coefficient decreased as the calcined kaolinite content of the calcined clay

increased and was about two orders of magnitude lower for LC^3-50 (95.0%) compared to PC system. While similar trends were obtained for the mortar and the paste samples, the apparent diffusion coefficients were generally higher for paste samples. This was likely to be due to the higher resolution of the μ-XRF, particularly in the surface region. A higher slope close to the surface gives higher values of the apparent chloride diffusion coefficient. Moreover, the presence of sand particles in mortars produces a dilution effect that decreases the overall porosity and transport properties relative to the neat pastes.
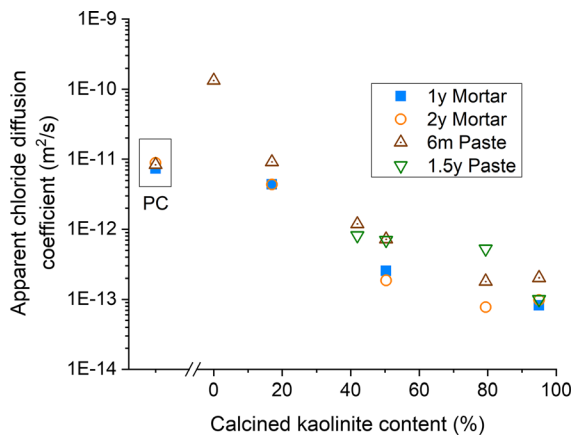
Fig. 5 Apparent diffusion coefficients for PC and LC^3-50 mortar and paste samples, calculated using Fick's law of diffusion

3.3 Porosity of PC vs LC^3-50 paste

Porosity characteristics obtained using MIP analysis of PC and LC^3-50 pastes are presented in Fig. 6 for the sample exposed to either water or 2 M NaCl solution for 6 months. A similar critical pore entry size is observed for PC and LC^3-50 (17.0%). The porosity observed for LC^3-50 (50.3%) and (95.0%) is significantly finer compared to PC samples. Similar results were obtained after 1.5 y of exposure. Moreover, interaction of the binders with chloride ions did not significantly affect the porosity. The trend in the ponding test results is in good agreement with the measured pore structure, i.e. the finer the pore connectivity, the more resistant the cementitious system to chloride ingress.

3.4 Chloride binding

The binding of chloride ions in different hydrates, specifically C–A–S–H and AFm phases slows down chloride ingress and delays the onset of reinforcement corrosion in concrete structures. The binding isotherm curves for PC, LC^3-50 and PPC-30 pastes are plotted in Fig. 7a and b. Figure 8 shows how the chloride binding varied with calcined kaolinite content in LC^3-50 and PPC30 paste systems at different NaCl concentrations. The binding of LC^3-50 blends varies with the calcined kaolinite content of calcined clay. There is a maximum of binding for blends containing clays with 40–80% of calcined kaolinite. For this
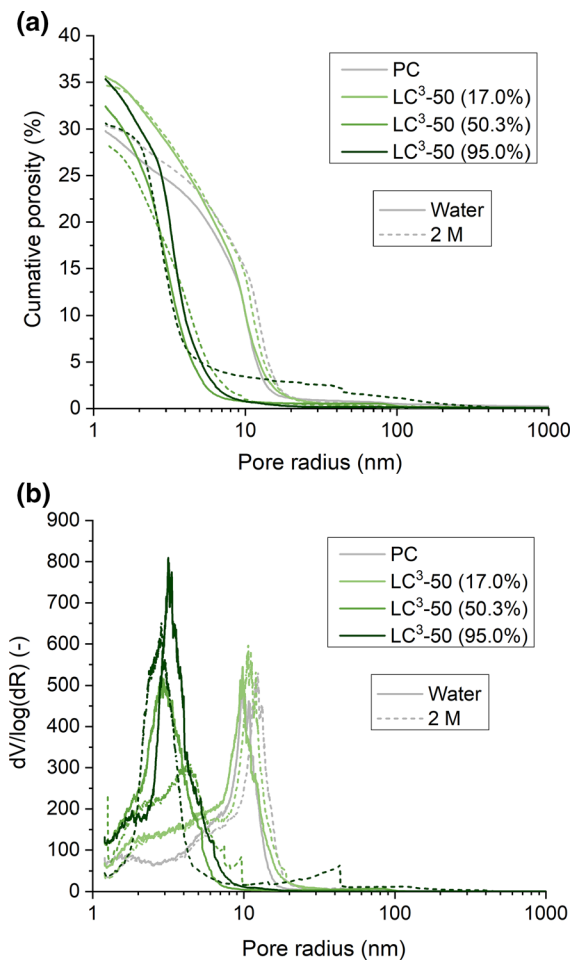
Fig. 6 Porosity distribution of PC and LC3-50 (17.0%), (50.3%) and (95.0%) paste samples after 6 m exposure to water or 2 M NaCl solution

range of calcined kaolinite content, the binding is higher for LC^3-50 blends than PC at 1 M and 2 M concentrations. Similar trends are observed for PPC30 blends, i.e. more chloride is bound in PPC-30 (41.9%) than PPC-30 (95.0%). However, there is no general trend for a higher or lower binding capacity of LC^3-50 compared with PPC30.

The vertical line in Fig. 7a indicates the concentration of the solution used in the ponding experiments of this study. At the concentration of the ponding test (0.51 M NaCl solution), the chloride binding was very similar for PC and the LC^3-50 blends with 40–50% of calcined kaolinite. The concentrations measured for ponding test at the top surface from Fig. 4a were added in Fig. 8. The results are globally in agreement with the binding results at 0.5 M NaCl, showing that the
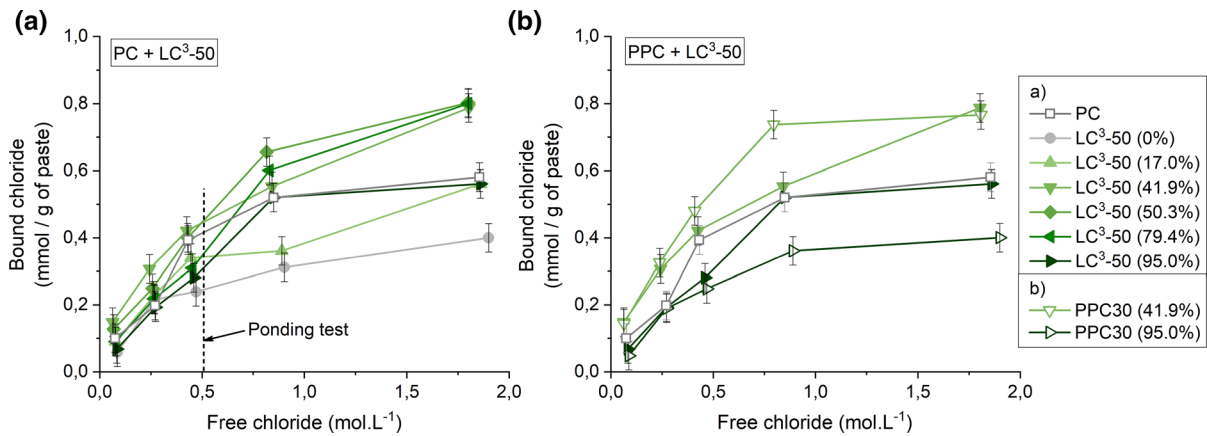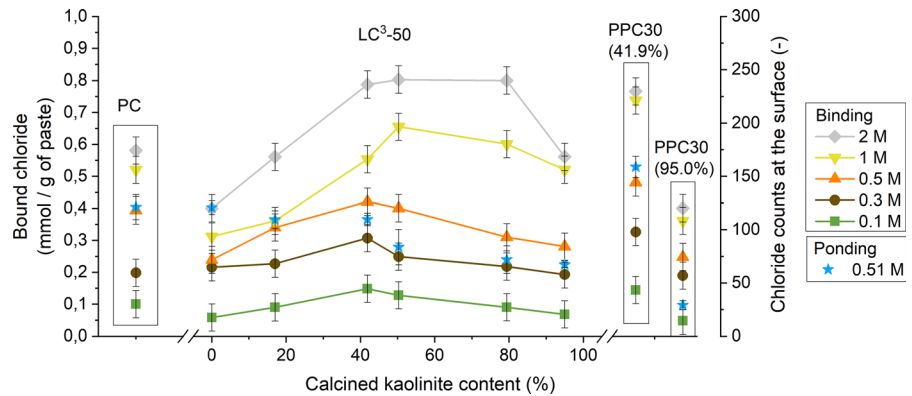
Fig. 7 Binding isotherm curves for LC^3-50 and PPC-30 pastes

Fig. 8 Total bound chloride as a function of clay grade in LC^3-50 and PPC30 pastes after exposure to 0.1 to 2 M NaCl solutions

concentration at the exposed surface is related to the binding capacity. The differences observed are mainly due to the scatter of μ-XRF measurements. For the binding isotherm test, the pH is lower than the pore solution of a normal concrete (excluding the approximately 200 μm-leached top layer of ponding sample). However, this pH variation does not seem to significantly impact chloride binding, as shown in supplementary material.

3.5 Phase assemblage and chloride distribution in hydrated phases

Quantification of the hydrates enables a better understanding of binding isotherm results. Figure 9a and b shows the amount of Friedel's salt, and carboaluminate phases in PC and LC^3-50 pastes, respectively. The amount of Friedel's salt is higher in LC^3-50 system containing calcined clays with 40–80% of calcined kaolinite, which originates from the higher

amount of carboaluminate phases in these systems. The more limited formation of carboaluminate hydrates for LC^3-50 with more than 50% of calcined kaolinite in calcined clay is explained by the lack of pores large enough in the microstructure for hydrate growth, as shown in [32]. This effect occurred at slightly higher calcined kaolinite content in this study because of the higher water to binder ratio used (0.5 versus 0.4). While some studies in the past tend to use high water/solid ratio perhaps to promote the degree of reaction of the cementitious components [e.g. 27], here the binding experiment was carried out on paste samples with w/s = 0.5. This can prevent full hydration of the solids (clinker and clay), yet has the advantage of better representing the real microstructure that develops in practical concretes. If higher water to solid ratio was allowed, the degree of reaction of clinker and clay would become higher, and this would result in higher binding capacity of the pastes.
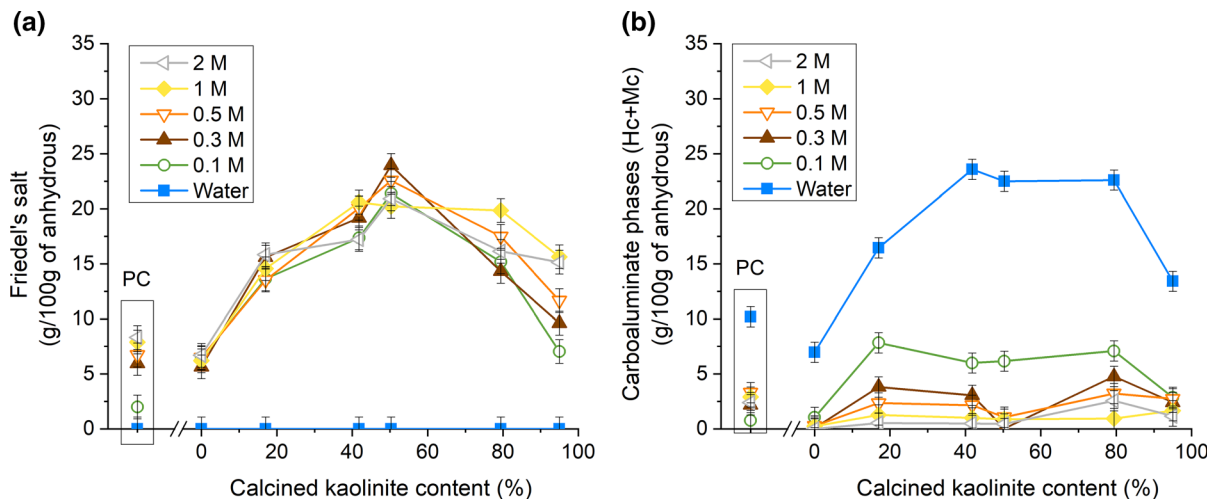
Fig. 9 Amount of Friedel's salt (**a**) and carboaluminate (**b**) phases in PC and LC³-50 pastes

Assuming that the bound chloride was distributed between only Friedel's salt and C–A–S–H, the amount of chloride adsorbed on C–A–S–H can be obtained as the difference between the total bound chloride (Fig. 7) and the amount of Friedel's salt (Fig. 9a). This distribution is shown in Fig. 10 for PC and the LC³-50 blends after exposure to 2 M NaCl solution. The determination of the chloride content in Friedel's salt at low NaCl concentrations (0.1 M, 0.3 M and 0.5 M) is challenging due to the coexistence of solid solutions of Mc (or Hc) and Friedel's salt [33]. This is

shown on XRD patterns of the pastes, available as supplementary material. The error for quantification of Friedel's salt in XRD was found to be ± 1.1 g Friedel's salt in 100 g of initial solid. The error for total bound chloride, measured using AgNO₃ titration was also found to be 0.05 mmol Cl per g of dried paste. These errors affected the bar charts, as indicated in Fig. 10.

4 Discussion

4.1 Chloride adsorption on C–A–S–H

These results suggest that the binding of chloride ions occurred both in Friedel's salt and on C–A–S–H. In LC³-50 pastes, more chloride was bound by Friedel's salt, whereas for the reference PC there was slightly more adsorbed on C–A–S–H. For PC, the lower initial amount of AFm phase was the reason for the lower formation of Friedel's salt.

To verify the extent of chloride adsorbed on C–A–S–H (i.e., Fig. 10), the amount of chloride adsorbed on C–A–S–H was calculated by measuring the chloride adsorption on C–A–S–H and by determining the amount of C–A–S–H. SEM–EDS analysis was used to measure the Cl/Ca ratio in C–A–S–H hydrates, after drying through solvent exchange method—which is assumed to remove the free, but not the chemically or physically bound chlorides. Figure 11 shows the atomic composition of the C–A–S–H for PC and
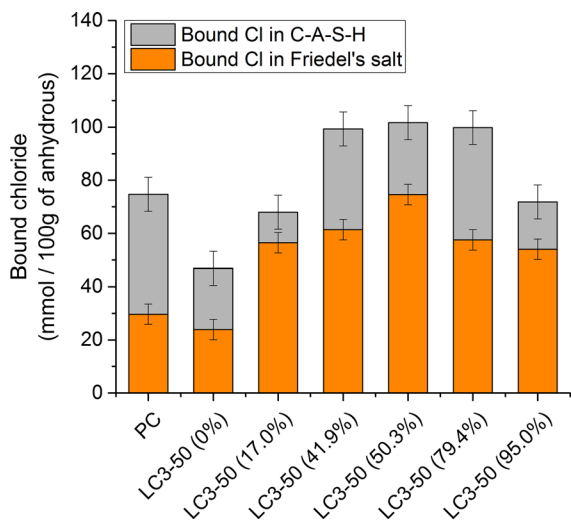

Fig. 10 Distribution of bound chloride between C–A–S–H and Friedel's salt in PC and in the different LC³-50 pastes after exposure to 2 M NaCl solution
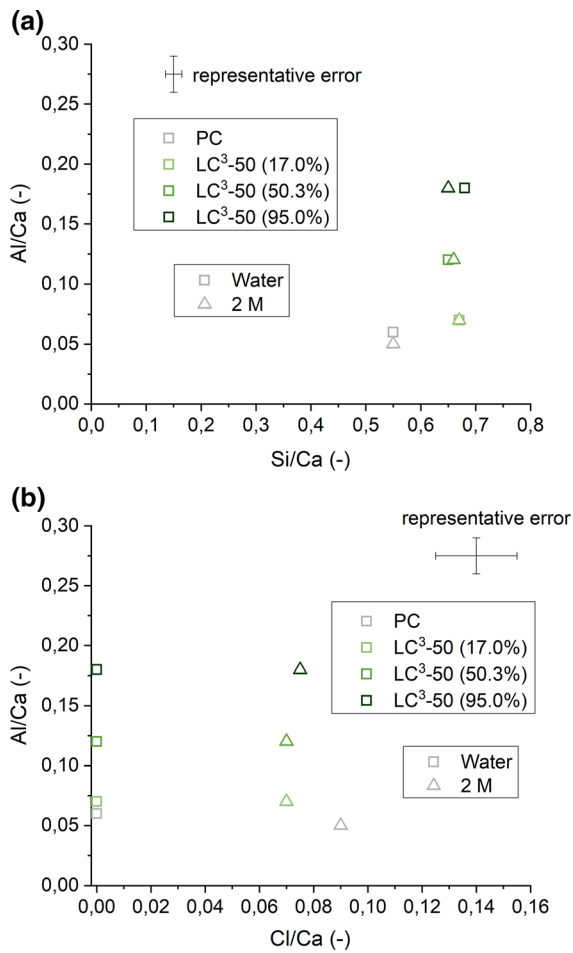
Fig. 11 SEM-EDS analysis of PC and LC³ pastes, **a** showing that the Si/Ca and Al/Ca of C–A–S–H stays intact after exposure to chloride ions, and **b** indicating binding of chloride in C–A–S–H after exposure to 2 M NaCl solution

LC³-50 (17.0%) (50.3%) and (95.0%) samples, after exposure to water or 2 M NaCl solution. The Al/Ca values are slightly lower and Si/Ca values are slightly higher than the values presented in [32] due to higher water to binder ratio used in this study (0.5 instead of 0.4). The interaction of the paste samples with chloride ions did not change the Al/Ca and Si/Ca of C–A–S–H as shown in Fig. 11a. However, significant chloride adsorption was observed for all samples stored in 2 M NaCl solution, as observed in Fig. 11b. The representative error corresponds to the least-intermixed C–A–S–H region from the cloud of 200 points collected for each sample.

The amount of C–A–S–H was determined for PC and LC³-50 blends by a coupled X-ray diffraction and

mass balance approach [34] which also permits the calculation of the reaction degree of metakaolin. The calculations of the amount of C–A–S–H, as well as the specific amount of chloride adsorption on C–A–S–H are available as supplementary material. The correlation of the amount of adsorbed chloride measured experimentally (using SEM–EDS analysis combined with mass balance) and calculated (difference of the total bound chloride and the chloride incorporated in Friedel's salt) is shown in Fig. 12. The dashed line indicates the ideal fit. A good correlation was obtained for PC and the LC³-50 (17.0%) and LC³-50 (50.3%) blends. Some deviation was observed for LC³-50 (95.0%) sample. This could be due to the difficulty of accurately quantifying Friedel's salt or measuring the Cl/Ca for this system due to the fine intermixing of metakaolin particles with C–A–S–H.

In general, it appears that there is higher specific absorption of chloride in the C–S–H in the PC system compared to the systems containing calcined clay, which are all similar.

4.2 Relative impact of binding and porosity refinement on chloride transport

In order to better understand the influence of binding and porosity on the ponding test results, the apparent chloride diffusion coefficient is compared in Fig. 13 to the amount of bound chloride at the same NaCl concentration (data from Fig. 8) and the critical pore
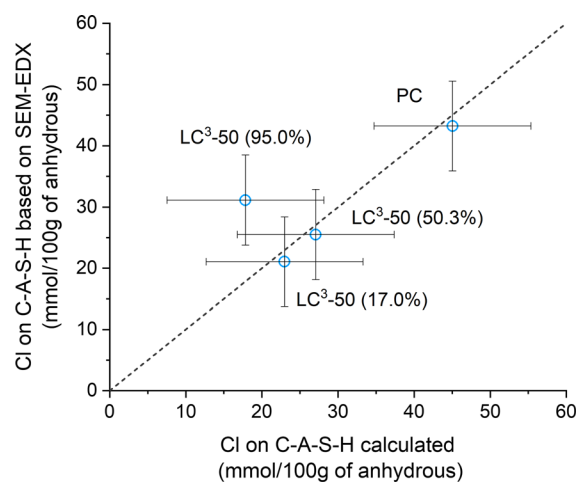

Fig. 12 Amount of adsorbed chloride on C–A–S–H determined experimentally by SEM–EDX and calculated as the difference of the total bound chloride and the chloride in Friedel's salt
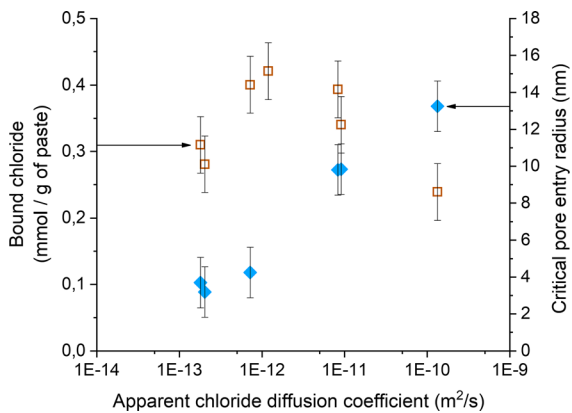
Fig. 13 Correlation between the bound chloride, the critical pore entry radius with the apparent chloride diffusion coefficient

entry radius obtained from the maximum of the derivative curve of MIP from Fig. 6b. It shows that the apparent chloride diffusion coefficient decreases with the decrease of the critical pore entry radius. There is no correlation between the amount of bound chloride and the apparent diffusion coefficient. Thus, at water to binder ratio of 0.5, the significant improvement of the chloride resistance obtained for the LC^3-50 systems seems not to be related to the difference of binding capacities, but more to the refinement of pore connectivity.

5 Conclusions

Use of calcined kaolinitic clays of various purity (i.e., kaolinite content) as a supplementary cementitious material was investigated with respect to chloride ion ingress at fixed water to binder ratio of 0.5. The following conclusions were drawn:

- When 30% or 50% of clinker was replaced by either only calcined clay (PPC-30) or by a combination of calcined clay and limestone (LC^3-50), excellent chloride ion transport resistance was achieved in mortar and paste mixtures, specifically with clays of around 40% and higher kaolinite content. The apparent diffusivity values were 1–2 orders of magnitude lower than PC.
- This improvement is mainly attributed to the refined pore structure of the mortars and pastes when calcined kaolinite clays were used rather than to changes in chloride binding capacity.

- Quantification of the phase assemblage of LC^3-50, before and after exposure to NaCl solutions indicated higher amount of carboaluminate AFm phases in LC^3-50 systems, resulted in formation of higher Friedel's salt. Nevertheless, as chloride binding also involved physical binding to C–A–S–H, the overall binding of chloride ions is not significantly different between LC^3-50 and PC systems.
- The amount of chloride binding to AFm and C–A–S–H was quantified, and it was concluded that while in PC, a larger portion of bound chloride goes to C–A–S–H, for LC^3-50 systems, most of the bound chloride was chemically fixed in Friedel's salt.

6 Supplementary material

6.1 XRD patterns of chloride binding isotherms

XRD Patterns of PC, LC^3-50 and PPC-30 pastes after 6 months of exposure to water and NaCl solutions (after 28 d of hydration) are shown in Fig. 14. The peak around 11.7 2θ° corresponds to Mc phase, which after exposure to NaCl of low concentration shifted towards lower angles, and by increasing the NaCl concentration shifted back to the theoretical position of pure Friedel's salt. The LC^3-50 (17.0%) system showed two peaks within 10.5–11.5 2θ°, at 0.1 M and 0.3 M NaCl solution exposure, indicating the coexistence of two phases, most probably Friedel's salt and a solid solution of Hc/Mc and Friedel's salt. Thus, obtaining the accurate amount of chloride bound to Friedel's salt was not straightforward at low NaCl concentrations.

6.2 Amount of C–A–S–H and specific chloride adsorption

Figure 15 shows that the amount of C–A–S–H increases with the calcined kaolinite content. Combining the results obtained in Figs. 11b, the normalized amount of adsorbed chloride on C–A–S–H can then be obtained (Fig. 16). The normalized chloride adsorption shows that PC has a higher specific binding capacity compared with LC^3-50 blends. There is no
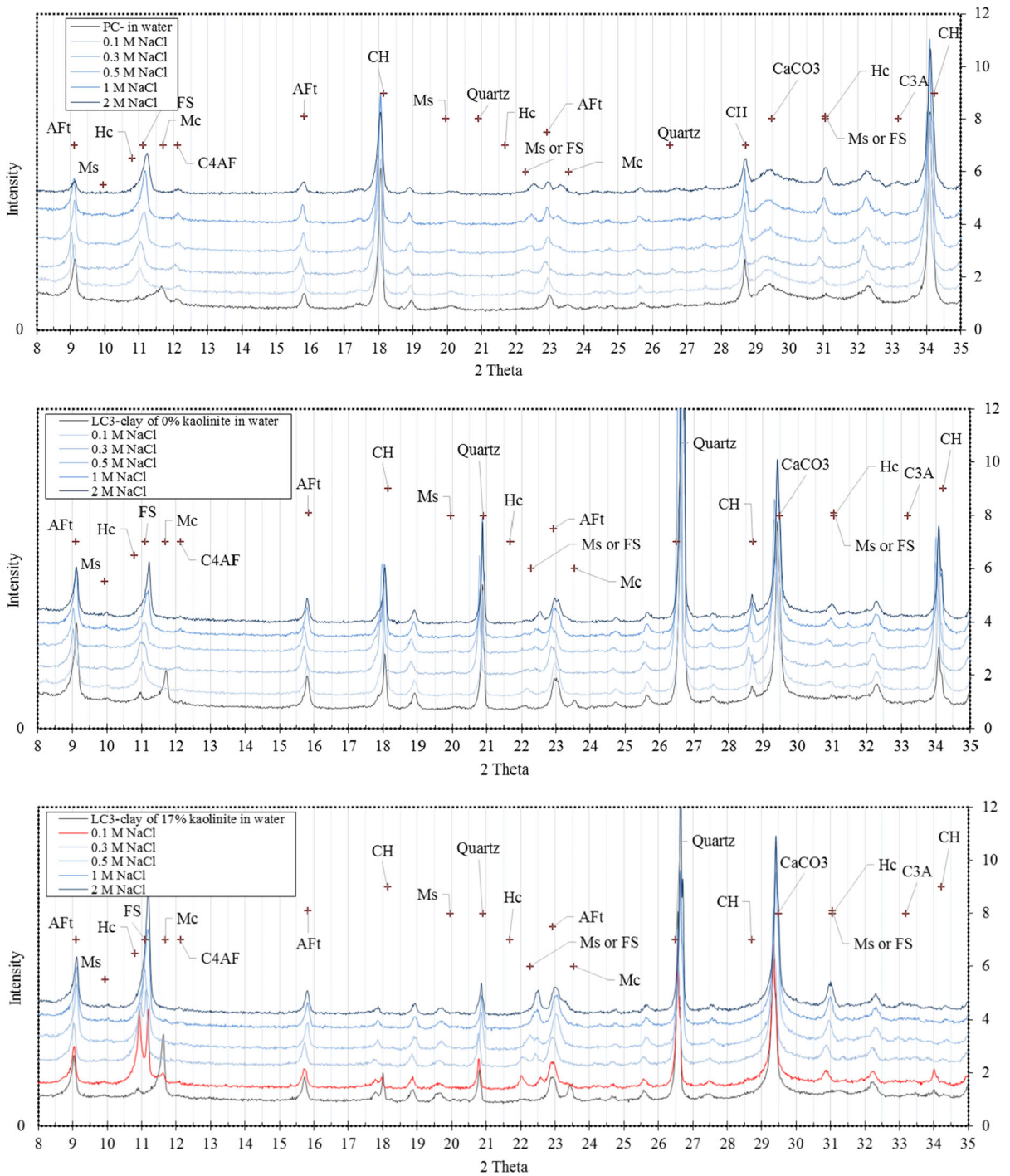
Fig. 14 XRD patterns of of PC, LC^3-50 and PPC-30 pastes after 6 months of exposure to water and NaCl
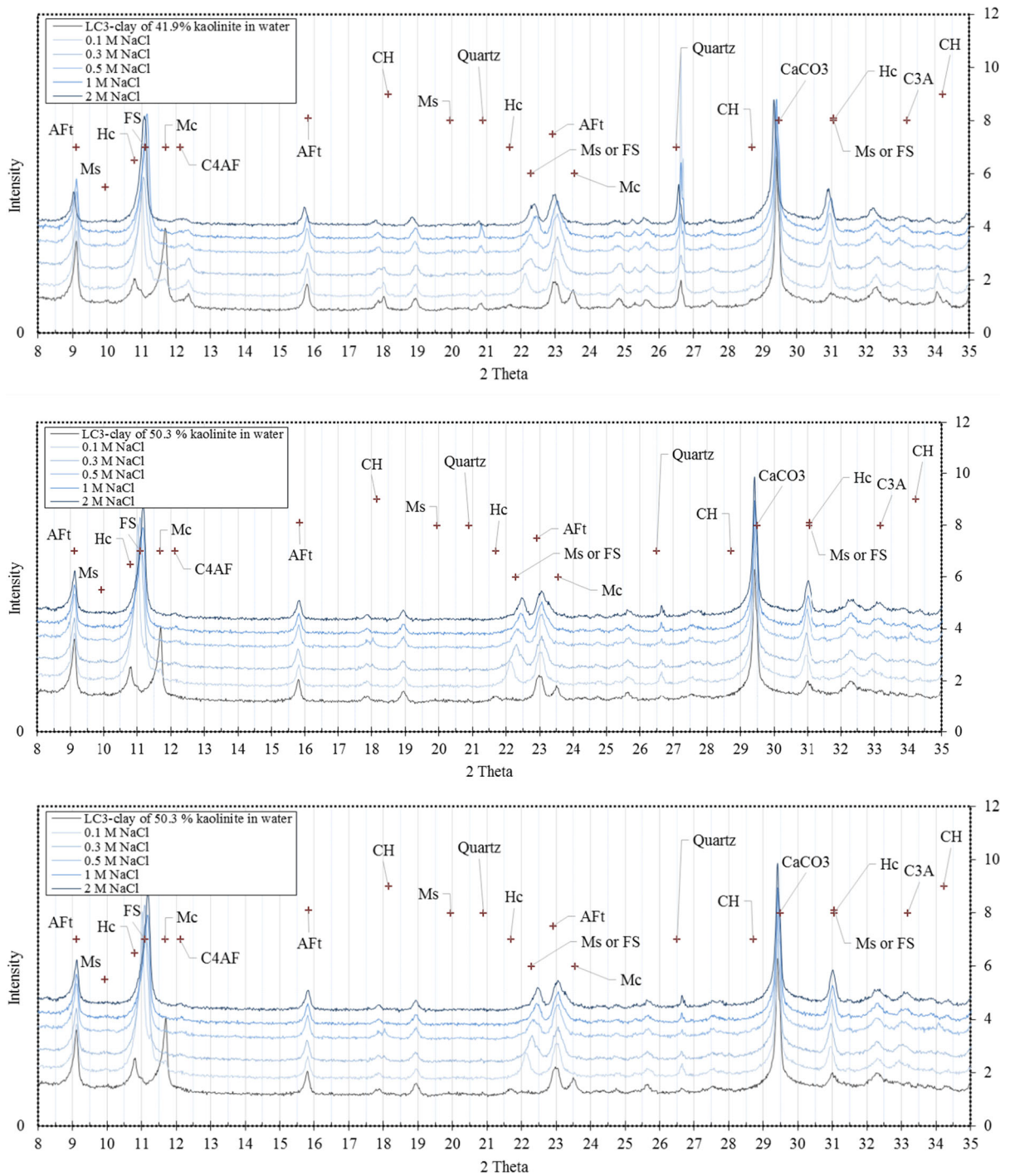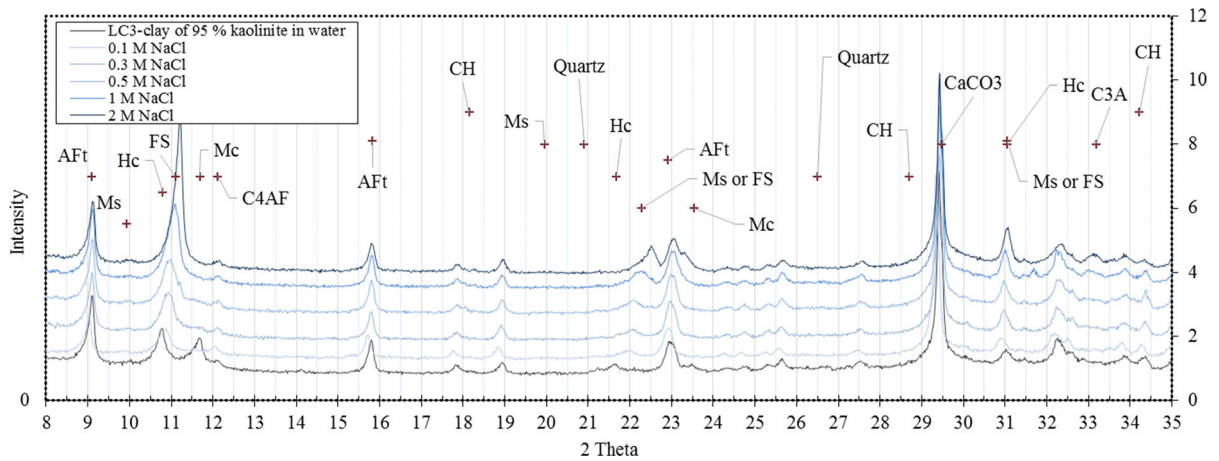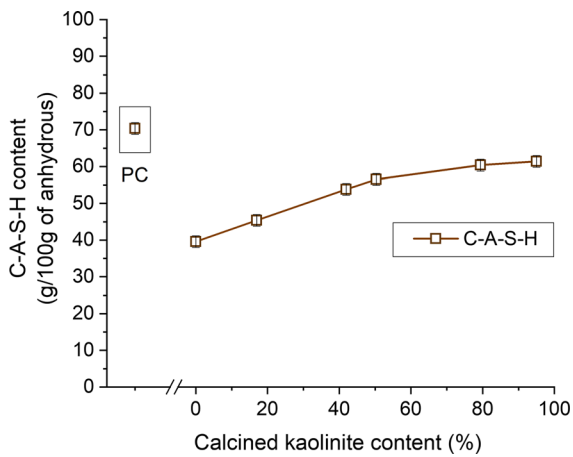
Fig. 14 continued

Fig. 14 continued

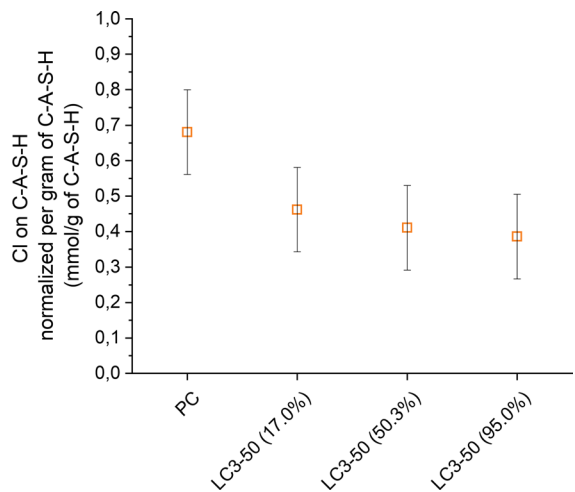**Fig. 15** Amount of C–A–S–H for PC and the different LC³-50 blends

Fig. 16 Chloride adsorption on C–A–S–H normalized per gram of C–A–S–H for PC and LC3-50 blends

clear influence of the calcined kaolinite content on the specific chloride adsorption of C–A–S–H.

6.2.1 Influence of environmental conditions during testing between ponding and binding isotherm tests

Due to the leaching of ions from the thin pieces of paste samples during the course of the binding experiment, the pH of the pore solution of the samples is expected to be lower than the pore solution of the samples subjected to ponding experiment. Figure 17 shows the comparison of pH values between binding and ponding conditions. The pH measured is about 1.5 point lower for binding sample.

In order to evaluate the influence of the pH on binding, the chloride adsorption on C–A–S–H was also measured for 0.5 M NaCl binding isotherm sample and 0.51 M NaCl ponding sample. For the ponding sample, the C–A–S–H composition was obtained at 5 mm below the exposed surface to ensure the microstructure was not impacted by leaching. The results in Fig. 18 shows that the chloride adsorption on C–A–S–H increases with concentration of the NaCl solution, and that similar chloride adsorption is observed for PC and for the LC³-50 blends. The small differences observed are in the range of error of the measurement. Thus, the change of pH had no significant impact on the chloride adsorption on C–A–S–H.
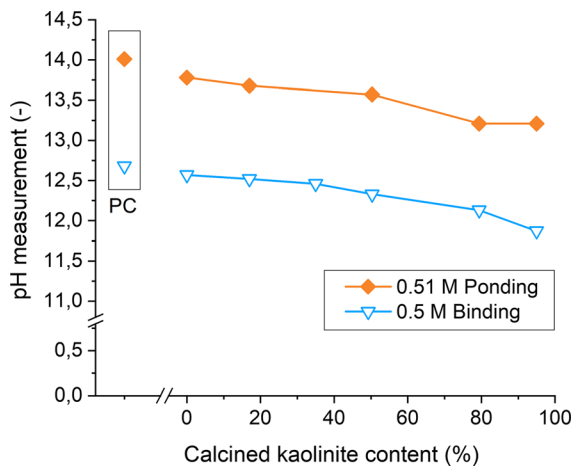
Fig. 17 pH measurement of ponding test and binding test for similar NaCl concentration
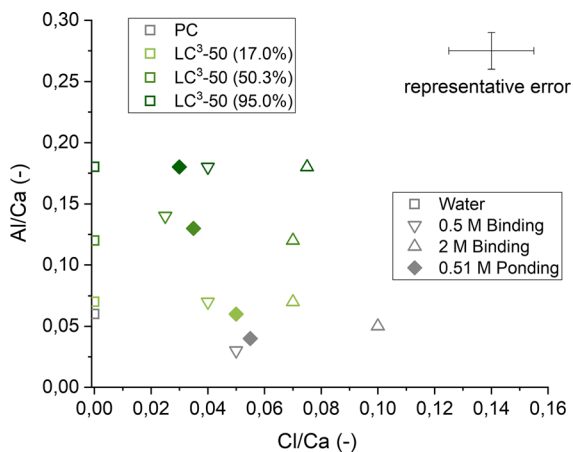

Fig. 18 Chloride adsorption on C–A–S–H measured by SEM–EDX for binding isotherm samples (in water, 0.5 M and 2 M NaCl) and ponding test samples (0.51 M NaCl)

Compliance with ethical standards

Conflict of interest The authors have declared that no conflict of interest exists.

Human and animal rights This article does not contain any studies with human participants or animals performed by any of the authors.

Informed consent Informed consent was obtained from all individual participants included in the study.

References

1. Scrivener K, John VM, Gartner EM (2016) Eco-efficient cements: Potential economically viable solutions for a low-CO2 cement-based materials industry. UNEP (United Nations Environment Program
2. Metz BD, Davidson O, Bosch P, Meyer L (2007) Contribution of Working Group III to the Fourth Assessment Report of the Intergovernmental Panel on Climate Change, in: C.U. Press (Ed.)
3. Global Soil Regions (2005) US Department of Agriculture—Natural Resources Conservations Service
4. Scrivener K, Favier A (Eds.) (2015) Calcined Clays for Sustainable Concrete: Proceedings of the 1st International Conference on Calcined Clays for Sustainable Concrete, Springer
5. Martirena F, Favier A, Scrivener K (2018) Calcined Clays for Sustainable Concrete: Proceedings of the 2nd International Conference on Calcined Clays for Sustainable Concrete, Springer
6. Avet F, Snellings R, Alujas Diaz A, Haha MB, Scrivener K (2016) Development of a new rapid, relevant and reliable (R3) test method to evaluate the pozzolanic reactivity of calcined kaolinitic clays. Cem Concr Res 85:1–11
7. Antoni M, Rossen J, Martirena F, Scrivener K (2012) Cement substitution by a combination of metakaolin and limestone. Cem Concr Res 42:1579–1589
8. Alujas A, Fernández R, Quintana R, Scrivener KL, Martirena F (2015) Pozzolanic reactivity of low grade kaolinitic clays: Influence of calcination temperature and impact of calcination products on OPC hydration. Appl Clay Sci 108:94–101
9. Fernandez R, Martirena F, Scrivener KL (2011) The origin of the pozzolanic activity of calcined clay minerals: a comparison between kaolinite, illite and montmorillonite. Cem Concr Res 41:113–122
10. Loser R, Lothenbach B, Leemann A, Tuchschmid M (2010) Chloride resistance of concrete and its binding capacity—comparison between experimental results and thermodynamic modeling. Cement Concr Compos 32:34–42
11. Arya C, Xu Y (1995) Effect of cement type on chloride binding and corrosion of steel in concrete. Cem Concr Res 25:893–902
12. Dhir RK, El-Mohr MAK, Dyer TD (1996) Chloride binding in GGBS concrete. Cem Concr Res 26:1767–1773
13. De Weerdt K, Colombo A, Coppola L, Justnes H, Geiker MR (2015) Impact of the associated cation on chloride binding of Portland cement paste. Cem Concr Res 68:196–202
14. Lothenbach B, Le Saout G, Gallucci E, Scrivener K (2008) Influence of limestone on the hydration of Portland cements. Cem Concr Res 38:848–860

15. Bonavetti VL, Rahhal VF, Irassar EF (2001) Studies on the carboaluminate formation in limestone filler-blended cements. Cem Concr Res 31:853–859

16. Thomas MDA, Hooton RD, Scott A, Zibara H (2012) The effect of supplementary cementitious materials on chloride binding in hardened cement paste. Cem Concr Res 42:1–7

17. Elakneswaran Y, Nawa T, Kurumisawa K (2009) Electrokinetic potential of hydrated cement in relation to adsorption of chlorides. Cem Concr Res 39:340–344

18. De Weerdt K, Orsáková D, Geiker MR (2014) The impact of sulphate and magnesium on chloride binding in Portland cement paste. Cem Concr Res 65:30–40

19. Zibara H, Hooton RD, Thomas MDA, Stanish K (2008) Influence of the C/S and C/A ratios of hydration products on the chloride ion binding capacity of lime-SF and lime-MK mixtures. Cem Concr Res 38:422–426

20. Dai ZT, Thuan T, Skibsted J (2014) Aluminum Incorporation in the C–S–H Phase of White Portland Cement-Metakaolin Blends Studied by 27Al and 29Si MAS NMR Spectroscopy. J Am Ceram Soc 97:2662–2671

21. Souri A, Kazemi-Kamyab H, Snellings R, Naghizadeh R, Golestani-Fard F, Scrivener K (2015) Pozzolanic activity of mechanochemically and thermally activated kaolins in cement. Cem Concr Res 77:47–59

22. De Weerdt K, Colombo A, Coppola L, Justnes H, Geiker MR (2015) Impact of the associated cation on chloride binding of Portland cement paste. Cem Concr Res 68:196–202

23. Shi Z, Geiker MR, Lothenbach B, De Weerdt K, Garzon SF, Enemark-Rasmussen K, Skibsted J (2017) Friedel's salt profiles from thermogravimetric analysis and thermodynamic modelling of Portland cement-based mortars exposed to sodium chloride. Cem Concr Compos 78:73–83

24. Badogiannis E, Aggeli E, Papadakis VG, Tsivilis S (2015) Evaluation of chloride-penetration resistance of metakaolin concrete by means of a diffusion e Binding model and of the k-value concept. Cement Concr Compos 63:1–7

25. Shekarchi M, Bonakdar A, Bakhshi M, Mirdamadi A, Mobasher B (2010) Transport properties in metakaolin blended concrete. Constr Build Mater 24:2217–2223

26. Boddy A, Hooton RD, Gruber KA (2001) Long-term testing of the chloride-penetration resistance of concrete containing high-reactivity metakaolin. Cem Concr Res 31(5):759–765

27. Shi Z, Geiker MR, DeWeerdt K, Østnor TA, Lothenbach B, Winnefeld F, Skibsted J (2017) Role of calcium on chloride binding in hydrated Portland cement–metakaolin–limestone blends. Cem Concr Res 95:205–216

28. Avet F, Snellings R, Alujas Diaz A, Haha MB, Scrivener K (2016) Development of a new rapid, relevant and reliable (R3) test method to evaluate the pozzolanic reactivity of calcined kaolinitic clays. Cem Concr Res 85:1–11

29. Moradllo MK, Sudbrink B, Hu Q, Aboustait M, Tabb B, Ley MT, Davis JM (2017) Using micro X-ray fluorescence to image chloride profiles in concrete. Cem Concr Res 92:128–141

30. F. Avet, Ph.D. Thesis, EPFL 2017

31. Rossen JE, Scrivener KL (2017) Optimization of SEM-EDS to determine the C–A–S–H composition in matured cement paste samples. Mater Charact 123:294–306

32. Avet F, Scrivener K (2018) Investigation of the calcined kaolinite content on the hydration of Limestone Calcined Clay Cement (LC3). Cem Concr Res 107:124–135

33. Balonis M, Lothenbach B, Le Saout G, Glasser FP (2010) Impact of chloride on the mineralogy of hydrated Portland cement systems. Cem Concr Res 40:1009–1022

34. Avet F, Scrivener K (2018) Investigation of the calcined kaolinite content on the hydration of Limestone Calcined Clay Cement (LC3). Cem Concr Res 107:124–135